THE ASTROPHYSICAL JOURNAL, 414:601–611, 1993 September 10

COMPARISON OF DISTRIBUTED REACCELERATION AND LEAKY-BOX MODELS OF COSMIC-RAY ABUNDANCES ($3 \leq Z \leq 28$)

JOHN R. LETAW
Severn Communications Corporation, 1023 Benfield Boulevard, Millersville, MD 21108; and
Department of Physics and Astronomy, Clemson University, Clemson, SC 29634-1911

REIN SILBERBERG
Universities Space Research Association, Suite 801, 300 D Street, SW, Washington, DC 20024

AND

C. H. TSAO
E. O. Hulburt Center for Space Research, Code 7654, Naval Research Laboratory, Washington, DC 20375
Received 1993 February 11; accepted 1993 March 12

ABSTRACT

A large collection of elemental and isotopic cosmic-ray data has been analyzed using the leaky-box transport model with and without reacceleration in the interstellar medium. Abundances of isotopes and elements with charges $3 \leq Z \leq 28$ and energies 10 MeV nucleon$^{-1} \leq E \leq 1$ TeV nucleon^{-1} were explored. Our results demonstrate that reacceleration models make detailed and accurate predictions with the same number of parameters, or fewer, as standard leaky-box models. Ad hoc fitting parameters in the standard model are replaced by astrophysically significant reacceleration parameters. Distributed reacceleration models explain the peak in secondary-to-primary ratios around 1 GeV nucleon^{-1}. They diminish the discrepancy between rigidity-dependent leakage and energy-independent anisotropy. They also offer the possibility of understanding isotopic anomalies at low energy (Silberberg et al. 1983).

Subject headings: acceleration of particles — cosmic rays — ISM: abundances

1. INTRODUCTION

Distributed reacceleration (DRAC) is a Galactic cosmic radiation transport model which includes acceleration by weak shocks occurring in supernova remnants. Charged ions and electrons at cosmic-ray energies above 10 MeV nucleon^{-1} are occasionally boosted to higher energies in these events. Both the frequency of shock encounters and the magnitude of energy increase are statistical distributions. These quantities may be related to other astrophysical observations. They are treated as free or fixed parameters in this analysis of cosmic-ray data.

DRAC models are similar to standard leaky-box models often used in the analysis of cosmic-ray data. Both models assume that cosmic radiation initially consists of energetic particles with a power-law distribution of momenta. The source composition is determined by relating transport results to cosmic-ray observations. Transport consists of approximately 10^7 yr of diffusive motion through the Galaxy during which nuclear spallation and decay significantly change the isotopic composition, ionization losses modify the energy spectra, and "Galactic escape" losses impose a distribution of path lengths.

It is likely that the regions through which cosmic rays pass contain shocks from supernovae (Blandford & Ostriker 1980; Eichler 1980). The shocks may alter cosmic-ray composition and energy spectra (Silberberg et al. 1983; Simon, Heinrich, & Mathis 1986). There are limits to this effect imposed by extensive observational data (Cowsik 1986); multiple strong shocks appear to be incompatible with observation.

In this paper we demonstrate the effect for nuclear species with $3 \leq Z \leq 28$ over a wide energy range from 10 MeV nucleon^{-1} to 1 TeV nucleon^{-1}. This range includes low energies where ionization losses and solar modulation are important. The objectives of this analysis follow.

The cosmic-ray interpretation problem is essentially of the form

$$\boldsymbol{Q} = \mathscr{L}(\boldsymbol{J}) \tag{1}$$

where $\boldsymbol{Q}$ is a vector of source abundances, $\mathscr{L}$ is a linear operator representing the modification of energy and composition as cosmic radiation passes through the Galaxy and heliosphere, and $\boldsymbol{J}$ is a set of energy spectra, one for each arriving nuclide. The quantities $\boldsymbol{J}$ are measured directly, and both $\mathscr{L}$ and $\boldsymbol{Q}$ are inferred from them in a self-consistent manner. The operator $\mathscr{L}$ is imperfectly known, hence there is no unique solution to equation (1). Excess freedom in the interpretation of cosmic-ray observations may be constrained by relating $\mathscr{L}$ to other astrophysical processes for which there are independent astrophysical observations. In particular, the reacceleration process is closely tied to the distribution and intensity of supernova shocks in the Galaxy.

A detailed, overall comparison of the standard leaky-box and DRAC models can resolve several issues. First, the acceptability of either model is established if a reasonable fit to the data is found. Second, the range of shock densities and intensities, if any, which are compatible with the data is determined. Third, by optimizing parameter choices in each model using numerical best-fit prodecures, the better data representation is identified.

Cosmic-ray transport models make specific predictions of isotopic and elemental abundances as a function of energy over a wide range. Differences between the predictions of DRAC and leaky-box models provide experimental signatures of the shock acceleration process.

Examination of goodness-of-fit criteria and parameter counts may also be of use in deciding which model is appropri-

ate for standard analysis of cosmic-ray data. In spite of the well-known richness of Galactic cosmic-ray transport theory (Ginzburg & Syrovatskii 1964), most experimenters analyze their data using essentially the standard leaky-box model described in this paper. Such an approach is justifiable because the simple model provides an adequate representation of the data. The DRAC model is a candidate for superseding standard analysis techniques because it replaces some arbitrary parameters with others which are physically motivated.

The numerical modeling performed here is unique in its comprehensive approach to the cosmic-ray transport problem. One or more of the essential components of our calculation have been omitted in all previous publications on reacceleration. These include (1) inclusion of a complete set of isotopes over a wide energy range, (2) ionization losses for proper treatment of low-energy components, (3) treatment of reacceleration events as stochastic processes that lead to a distribution of energies (Green's function method), (4) consideration of a realistic distribution of shock intensities in the ISM, and (5) use of established energy-dependent spallation cross sections to follow the transmutation of isotopes.

2. TRANSPORT METHODS

The process of transporting cosmic radiation from its source to the detector is shown schematically in Figure 1. Several distinct sets of parameters determine the *Galactic transport*. The *relative source abundances* are the amounts of each nuclide at the hypothetical cosmic-ray source. These abundances are roughly correlated with general abundances of isotopes in the solar system with a bias in favor of nuclides with low first-ionization potentials. The *atomic and nuclear data* include primarily nuclear spallation cross sections, but also nuclear decay diagrams, ionization loss rates, and electron stripping and attachment cross sections. The *astrophysical parameters* characterize the initial spectrum of cosmic radiation, the amount of material which it passes through, the average density of the material, and details of shock acceleration processes. Astrophysical parameters and source abundances are optimized to best fit the cosmic-ray observations; atomic and nuclear data may be established in terrestrial experiments. Further discussion of Galactic transport parameters is presented by Letaw, Silberberg, & Tsao (1984).

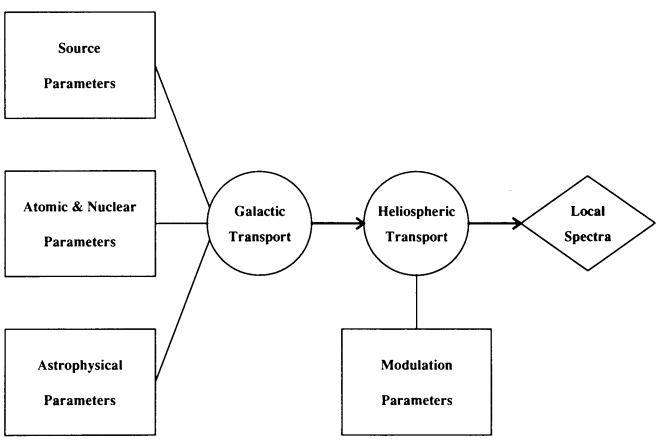

FIG. 1.—Schematic view of the cosmic-ray transport modeling in this paper. Rectangles enclose required parameter sets; circles enclose stages of transport; and the diamond encloses the results.

Galactic transport is undertaken using a one-dimensional continuity equation. The leaky-box model is adopted to simulate diffusion in a Galactic confinement region where particles have a certain probability of escape. The loss term is a simple loss probability which may be both energy- (or rigidity-) and species-dependent. The equation also contains terms representing ionization loss, nuclear spallation, formation of spallation products, both beta decay and electron capture decay, and acceleration by weak interstellar shocks. Standard leaky-box models contain no shock processes. When shocks are included, the models are called distribution reacceleration models because they intermingle acceleration with the other transport processes over the entire cosmic-ray path.

The differential equation used in this analysis follows Letaw & Roginsky (1989).

$$\frac{\partial J_i(E)}{\partial x} = \frac{Q_i(E)}{\rho} - r_i^e(E)J_i(E) + \frac{\partial}{\partial E}[\omega_i(E)J_i(E)] - r_i^s(E)J_i(E) + \sum_j r_{ij}^s(E)J_j(E) - r_i^d(E)J_i(E) + \sum_j r_{ij}^d(E)J_j(E) - r_i^{EC}(E)g_i(E)J_i(E) + \sum_j r_{ij}^{EC}(E)g_j(E)J_j(E) - r_i^a(E)J_i(E) + (\mu - 1)v^{-1}p^{-\mu}\int_0^E r_i^a(E')(p')^{\mu-1}J_i(E')dE' = 0 . \quad (2)$$

In equation (2) the $J_i(E)$ are differential energy spectra representing the flux of nuclei of species i at energy E. The rate of change over a path length, x, is set to zero, implying that cosmic radiation is in equilibrium in the Galaxy. $Q_i(E)$ is the source injection term, and ρ is the interstellar medium (ISM) density. Terms $r_i(E)$ are rates for various processes indicated by superscripts e (escape), s (spallation), d (particle decay), EC (electron-capture decay), and a (acceleration); $\omega_i(E)$ is the energy-dependent stopping power of species i in the ISM. Terms $r_{ij}(E)$ represent increases in species i resulting from losses in species j. The factor $g_i(E)$ accounts for the portion of cosmic radiation which is fully ionized and unable to decay by electron capture (Letaw et al. 1985). For simplicity, helium and ionized hydrogen components of the ISM are not included in this analysis.

The reacceleration effect is modeled in the last two terms. It is a Green's function which transforms a delta function in momentum $[\delta(p - p')]$ into a power law in momentum $(p^{-\mu})$ while preserving particle number. A single shock strength is parameterized by μ; a realistic distribution of shock strengths requires several terms of the same form with different values of μ. Figures 2 and 3 show the effect of a single shock encounter on a monoenergetic particle spectrum. In principle, the Green's function could be more complicated. For example, no provision is made here for particle deceleration or for energy dependence in the Green's function shape.

There is a direct connection between the shock strength μ and the compression ratio R and Mach number M of interstellar shocks. For planar shocks, $\mu = (2 + R)/(R - 1)$ and $R = 4M^2/(3 + M^2)$. Studies in interplanetary and solar environments validate the mechanisms which are here extended to the ISM. When these models are applied to supernova bursts, specific predictions about both the distribution

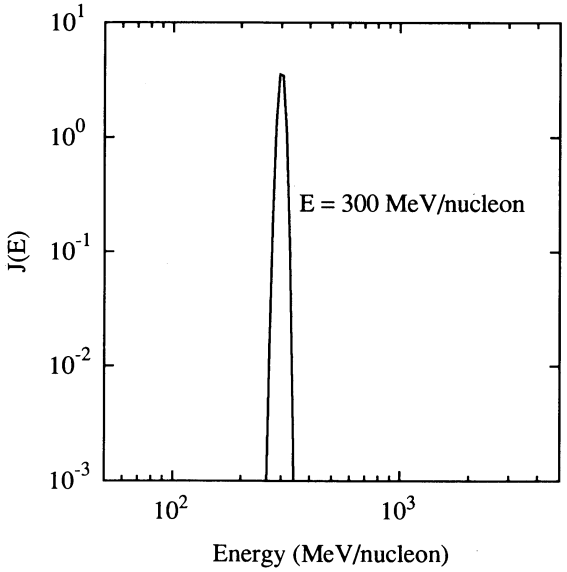

FIG. 2.—Monoenergetic cosmic-ray spectrum *before* interaction with weak interstellar shocks. Cosmic-ray energy is 300 MeV nucleon^{-1}.

and the intensity of ISM shocks are possible (Axford 1981). Our transport modeling demonstrates that the deduced distribution is consistent with the cosmic-ray composition, thereby providing additional validation of supernova models.

The weighted-slab model, an alternative to the leaky-box model, is also widely used for cosmic-ray data analysis. In that model cosmic radiation is transported through a series of different thicknesses, or "slabs." The results are then weighted according to an arbitrary path-length distribution and summed. The transport equation specifically excludes the escape probability, but could include reacceleration.

Weighted-slab and leaky-box models are equivalent when energy-changing processes (ionization loss and reacceleration) are not present and when the exponential path-length distribution is used. In general the two approaches yield different

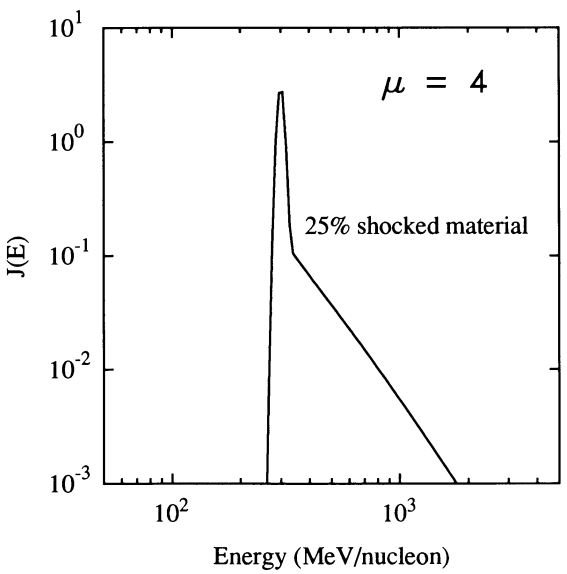

FIG. 3.—Resulting spectrum *after* 25% of the material in Fig. 2 has been accelerated in an interstellar shock with index $\mu = 4$.

results (Jones 1991). Lezniak (1979) has shown that the weighted-slab model is inconsistent with a generalized three-dimensional diffusion equation.

Accurate fits to secondary-to-primary ratios are facilitated in the weighted-slab model because the mean path length at each energy is chosen to fit the boron/carbon (B/C) ratio at that energy. These adjustments of the functional form of the path-length energy dependence are otherwise unconstrained. We do not use the weighted-slab model here because the arbitrary path-length distribution function imparts far more parametric freedom than is needed to produce an adequate fit to the data. Neither the standard leaky-box nor the DRAC models require so many parameters.

Galactic transport is essentially determined by 10 astrophysical parameters defined in the following equations. Several of the standard leaky-box model parameters have little or no theoretical justification. They have been introduced only to provide closer agreement between the model and observational data. We call these ad hoc parameters here, because they are introduced specifically for fitting purposes. It is one of the aims of the DRAC model to replace these parameters with others having a closer connection to astrophysical observations.

The source spectrum is a power law in momentum with index Γ ($\Gamma < -2$) at high energy. This spectrum is generated when particles are accelerated by a single, very intense shock. A power of velocity (β^{κ}) can be included to flatten the source spectrum at low energy. Our flattening factor emulates other flattening functions, for example, the familiar (total energy + 400 MeV nucleon^{-1}) term. These flattened source spectra are used in standard leaky-box model analyses to improve the fit to primary particle spectra such as oxygen. The factor κ is ad hoc as defined above. If the source spectrum is considered to be a function of momentum, not kinetic energy per nucleon, then κ should be increased by 1.

$$\text{Source spectrum shape } [(\text{MeV nucleon}^{-1})^{-1}] = \beta^{\kappa} p^{\Gamma} . \quad (3)$$

The mean escape path length is a power law in rigidity with index ε ($\varepsilon < 0$) above a threshold rigidity R_c. The mean escape path length is normalized to λ_c at $R = 10$ GV. Below the rigidity threshold the path length is proportional to β^{ν}, with the constant of proportionality determined by matching the two functions at the threshold. The parameters R_c and ν are ad hoc, but may have some theoretical basis in convection transport theory (Jokipii 1976; Jones 1979). R_c and ν are not needed and not used in DRAC models.

$$\text{Mean escape path length (g cm}^{-2}) \begin{cases} = \lambda_e (R/10)^{\varepsilon} , & R > R_c , \\ \propto \beta^{\nu} , & R \le R_c . \end{cases} \quad (4)$$

The mean reacceleration path length is a power law in rigidity with index α ($\alpha \ge 0$). The path length is normalized to λ_a at $R = 10$ GV. The function form was chosen arbitrarily. It is similar to the escape path-length function. The mean reacceleration path length is not used in conventional leaky-box models.

$$\text{Mean reacceleration path length (g cm}^{-2}) = \lambda (R/10)^{\alpha} . \quad (5)$$

The shock strength describes the effect of shock on a particle spectrum. A monoenergetic spectrum is changed into a power law in momentum with index $-\mu$ by the shock. Here μ is not used as a fitting parameter; it is used to describe the range of

solutions which occur with different shock strengths. Within broad restrictions, i.e., not too many shocks with $\mu < 3$, any value of μ can yield an acceptable fit (Wandel et al. 1987). The actual values used in data analysis comprise a distribution which can be described independently of the cosmic-ray data (see, for example, Axford 1981):

$$\text{Shock strength} = \mu \, . \tag{6}$$

The mean hydrogen density coupled with the escape path length determines the cosmic-ray confinement time, and hence the abundances of unstable species such as ^{10}Be. The density represents the mean density encountered by cosmic rays and is not necessarily equal to the density of the ISM in the Galaxy. We have adopted the fixed value $\rho = 0.3$ atoms cm^{-3} (Wiedenbeck & Greiner 1980; Garcia-Munoz, Simpson, & Wefel 1981). Variation of the density can improve the fit to several isotopic ratios, but has an inconsequential effect on simultaneous fits to the entire set of cosmic-ray observations:

$$\text{Mean hydrogen density (atoms cm}^{-3}) = \rho \, . \tag{7}$$

We define four different models based on the parameters which are optimized to fit the cosmic-ray observations. These are shown in Table 1. Eight of the 10 parameters described above are free to be optimized. The ISM density (ρ), and the shock strength (μ) or shock-strength distribution [$f(\mu)$] are fixed. DRAC model 1 is closest in spirit to our previous work (Silberberg et al. 1983; Wandel et al. 1987) and that of other research (e.g., Simon et al. 1986; Stephens 1990). The reacceleration rate in model 1 is energy-independent. DRAC models 2 and 3 differ from earlier models. The reacceleration rate declines with increasing energy. The standard leaky-box model has no reacceleration.

Standard leaky-box models use six parameters, including two defining spectral shape and four defining the mean Galactic escape path length. The DRAC models require either five or six parameters. The additional reacceleration parameters do not increase the overall parameter count because DRAC models do not need and do not use the low-rigidity flattening of the escape path length (R_c, ν) to fit observations. Model 2 has one fewer parameter because the spectral flattening κ is not used.

The *heliospheric transport* phase is modeled using the force-field approximation to solar modulation proposed by Gleeson & Axford (1968). Modulation is represented by a solar-activity–dependent effective potential of several hundred megavolts (MV). The *modulation parameters* consist of several potentials, Φ_I, one for each data set/observation period. Other modulation models exist, for example, the Fisk (1971) spherical diffusion model. We expect that such models offer only a small improvement on the predictive capability of heavy-ion transport models, but look forward to testing this assumption in future studies.

We note that solar modulation affects low-energy cosmic radiation most intensely. Particles with energies less than a few hundred MeV nucleon^{-1} outside the heliosphere are stopped before reaching Earth. Low-energy processes are therefore effectively hidden from view. Furthermore, the precise effect of modulation can only be known when spectra inside and outside the heliosphere are measured independently. The outside spectrum of heavy ions has not yet been measured. Since the reacceleration process, as well as any flattening of the source spectrum, alters the predicted low-energy spectral shape outside the heliosphere, an adjustment of previously derived modulation parameters may be required to maintain consistency between DRAC models and the observations.

TABLE 1

SUMMARY OF TRANSPORT MODELS INVESTIGATED IN THIS PAPER

Model	Fitted Parameters	Fixed Parameters
Standard	$\Gamma, \kappa, \lambda_e, \varepsilon, R_c, \nu$	$1/\lambda_a = 0, \alpha = 0$
Reacceleration 1	$\Gamma, \kappa, \lambda_e, \varepsilon, \lambda_a$	$R_c = 0, \nu = 0, \alpha = 0$
Reacceleration 2	$\Gamma, \lambda_e, \varepsilon, \lambda_a, \alpha$	$\kappa = 0, R_c = 0, \nu = 0$
Reacceleration 3	$\Gamma, \kappa, \lambda_e, \varepsilon, \lambda_a, \alpha$	$R_c = 0, \nu = 0$

3. DATA SELECTION AND FITTING

In this section the transport model described in § 2 is used to analyze a comprehensive set of cosmic-ray observations. The analysis is performed numerically using the cosmic-ray transport code CTX 2.0 (Letaw 1992) and auxiliary programs. Our technique obtains best fits of the astrophysical parameters and relative source abundances. The resulting local spectra are intercompared, both quantitatively using a goodness-of-fit measure and visually using graphs of various abundance ratios, to answer questions set forth in the Introduction.

The CTX 2.0 code, as utilized in this paper, follows the transport of 81 nuclides from Li ($Z = 3$) through Ni ($Z = 28$). The spectrum of each nuclide is represented at 100 energies logarithmically distributed from 10 MeV nucleon^{-1} to 1 TeV nucleon^{-1}, i.e., at 20 points per decade. In terms of equation (1), $\boldsymbol{Q}$ is a vector with 8100 elements containing the source parameters (relative source abundances) as well as the source spectrum shape. $\mathscr{L}$ is represented by an 8100 × 8100 matrix containing all atomic and nuclear data, astrophysical parameters (except source spectrum shape), and modulation parameters. The local spectra, $\boldsymbol{J}$, also form an 8100 element vector and are obtained by finding

$$\boldsymbol{J} = \mathscr{L}^{-1}(\boldsymbol{Q}) \, . \tag{8}$$

The best-fit procedures described here require a set of observational cosmic-ray abundance data with error estimates. We have selected 489 data points from nine experiments. The data were chosen to represent the wide range of energies and nuclides covered by our model. Both elemental and isotopic data were selected with emphasis on including at least one datum for each nuclide. References for the nine data sets are shown in Table 2. Note that the abundance and error for ^{47}Ti in Webber (1981) were increased by a factor of 1.5 to correct a typographical error in that reference. Recent, and more precise, isotopic data for iron and sub-iron nuclei (Leske, Milliken, & Wiedenbeck 1992) were not available when this research was performed.

Most of the data are abundance ratios, and many of those ratios are reported relative to the elemental abundance of oxygen. To ensure that absolute spectra are properly represented, we have included the absolute oxygen intensities reported in data sets 1, 5, and 6. In order to attain consistent results, all output spectra are normalized so that the flux of oxygen at 20 GeV nucleon^{-1} is 5.96×10^{-3} m^{-2} s^{-1} sr^{-1} (GeV nucleon^{-1})$^{-1}$. This normalization factor was found by performing a least-squares fit to data in data set 1 at 10.6, 16.2, and 35.0 GeV nucleon^{-1} and data set 6 at 72.6, 102.6, and 206.8 GeV nucleon^{-1}.

TABLE 2

REFERENCES TO OBSERVATIONAL DATA

Set	References	Data Points
1.....	Engelmann et al. 1990 Ferrando et al. 1988	331
2.....	Binns et al. 1988	11
3.....	Ferrando et al. 1991	12
4.....	Wiedenbeck & Greiner 1980 Wiedenbeck 1983 Wiedenbeck 1985 Krombel & Wiedenbeck 1985 Krombel & Wiedenbeck 1988	10
5.....	Garcia-Munoz et al. 1981 Garcia-Munoz & Simpson 1979 Garcia-Munoz et al. 1979	33
6.....	Swordy et al. 1990 Muller et al. 1991	20
7.....	Gupta & Webber 1989	11
8.....	Webber et al. 1985	29
9.....	Webber 1981	32

For purposes of comparing the local spectra predicted by the models with observed cosmic-ray abundances, we have defined a convenient goodness-of-fit measure similar to the χ^2 statistical measure:

$$\text{Goodness of fit} = \sum_j \frac{(P_j - X_j)^2}{(w_j \delta X_j)^2} . \quad (9)$$

X_j is an observed abundance or abundance ratio, δX_j is the uncertainty or error in X_j, and P_j is the value of X_j predicted by the transport model; w_j is the weighting factor used to deemphasize some data sets in the fitting process by increasing the statistical errors. It is discussed further below.

In principle the goodness-of-fit measure could be used as the basis for statistical analysis of the model. The goodness-of-fit measure should be distributed according to a χ^2 distribution. In practice, sources of unquantified errors limit the usefulness of this interpretation. They are systematic errors in (1) semiempirical cross-section formulae and (2) published cosmic-ray observations. We believe that the goodness-of-fit measure is useful for optimizing parameters of each transport model and for rank-ordering the fidelity of several different transport models. We use the same goodness-of-fit measure to interpret both standard and DRAC models.

To obtain the best fit to observational cosmic-ray data using standard transport codes, one must perform the following steps:

Step 1: Guess the unknown parameters.
Step 2: Run the program to find $J_i(E)$.
Step 3: Compute the goodness of fit relative to observational data.
Step 4: Modify parameters based on goodness of fit and visual analysis of data.
Step 5: Go to step 2 until the best fit is obtained.

This method is unsatifactory because there is no criterion for assessing when the best fit has been achieved. Furthermore, each step requires manual intervention, which significantly slows the calculation.

We have devised several methods for minimizing the goodness-of-fit measure relative to each of the parameter sets above (source, modulation, astrophysical). The approaches for each are specialized. For example, the arriving abundances are linearly related to the source abundances, so that for fixed astrophysical parameters and transport model the entire interstellar transport may be summarized in a matrix with dimensions 8100 × 81 [length of $J_i(E)$ multiplied by the number of relative source abundances]. The fitting procedure is nonlinear; however, the iterative process now involves only a large matrix multiplication.

This method was used to obtain the source abundances (Table 3) which are used in all remaining calculations. A few of the secondary abundances are quite different from what is expected based on solar system abundances. The nature of the fitting process compensates for small cross-section errors by altering the source abundances. For example, since the cross section σ ($^{56}\text{Fe} \rightarrow {}^{52}\text{Cr}$) is a few percent low, a large apparent source abundance of ^{52}Cr is required to make up the discrepancy with observational data. Careful propagation of cross-section and observational errors reveals that these differences are not statistically significant. Secondary source abundances with large errors are bracketed in Table 3.

Other fits in this study were obtained by simultaneously varying the astrophysical and modulation parameters. The computational procedure utilizes multidimensional, nonlinear, least-squares fitting (Press et al. 1986) to find values of five or six astrophysical parameters. One-dimensional techniques provide optimized modulation parameters. The technique also yields the goodness-of-fit measure for each model measured against the observational data sets.

Our initial fits to the data were unsatisfactory. For example, the best-fit standard model calculation was found to have a goodness of fit of 1786 with 489 data points. This corresponds to $\chi^2/\text{DOF} \approx 4$, much higher than the value of unity required for a good model. A careful review of the results leads us to attribute some of the discrepancy to semiempirical cross-section uncertainties and some to systematic errors in the cosmic-ray data sets. All residuals greater than 3.5 standard deviations occurred in data sets 1, 8, and 9. We have deemphasized these data sets in the remaining fits by applying weighting factors of 1.8 to errors in data set 1, and 2.0 to errors in data sets 8 and 9.

We do not believe inclusion of the weighting factors affects the validity of our analysis. They serve only to emphasize some data sets at the expense of others. Including weighting factors renders useless the statistical significance of χ^2. Consequently, we use the goodness-of-fit measure only as a relative indicator of fidelity to observational data.

4. RESULTS

The transport code runs were designed so that standard and DRAC models could be compared on an equal footing. All free astrophysical and modulation parameters are optimized relative to the observational data. The remaining parameters are held fixed at the same constant values for all runs. Remaining parameters include the source abundances (Table 3), the atomic and nuclear data (§ 2), the ISM density (0.3 atoms cm^{-3}), and the transport equation (eq. [2]).

The shock strength parameter (μ) is a single, fixed constant in most runs, so that fit sensitivity to encounters with various shock intensities can be described. We have also performed runs with a distribution of shock strengths, $f(\mu)$, which is taken

TABLE 3

COSMIC-RAY SOURCE ABUNDANCES ($^{16}O \equiv 10^6$)

Nuclide	Abundance	Nuclide	Abundance	Nuclide	Abundance
^{6}Li	[2.42×10^{-1}]	^{30}Si	[5.53×10^{2}]	^{48}Ti	[9.67]
^{7}Li	[3.02]	^{31}P	[9.81×10^{2}]	^{49}Ti	[7.17×10^{-1}]
^{7}Be	(unstable)	^{32}S	2.41×10^{4}	^{50}Ti	[6.96×10^{-1}]
^{9}Be	[6.52×10^{-2}]	^{33}S	[2.45×10^{2}]	^{49}V	(unstable)
^{10}Be	(unstable)	^{34}S	[1.15×10^{2}]	^{50}V	[3.32×10^{-2}]
^{10}B	[9.78×10^{-2}]	^{36}S	[3.70×10^{-1}]	^{51}V	[6.88×10^{1}]
^{11}B	[3.92×10^{-1}]	^{35}Cl	[1.95×10^{1}]	^{48}Cr	(unstable)
^{12}C	8.65×10^{5}	^{36}Cl	(unstable)	^{50}Cr	[2.97]
^{13}C	[1.45×10^{4}]	^{37}Cl	[6.30]	^{51}Cr	(unstable)
^{14}C	(unstable)	^{36}Ar	3.06×10^{3}	^{52}Cr	[2.44×10^{3}]
^{14}N	6.30×10^{4}	^{37}Ar	(unstable)	^{53}Cr	[2.34×10^{2}]
^{15}N	[2.31×10^{3}]	^{38}Ar	[9.08×10^{1}]	^{54}Cr	[8.21×10^{1}]
^{16}O	1.00×10^{6}	^{40}Ar	[1.09×10^{-3}]	^{53}Mn	(unstable)
^{17}O	[8.82×10^{1}]	^{39}K	[1.77×10^{1}]	^{54}Mn	(unstable)
^{18}O	[2.04×10^{2}]	^{40}K	[2.60×10^{-1}]	^{55}Mn	[5.05×10^{1}]
^{19}F	[4.24]	^{41}K	[1.31]	^{54}Fe	[1.15×10^{4}]
^{20}Ne	9.19×10^{4}	^{40}Ca	1.18×10^{4}	^{55}Fe	(unstable)
^{21}Ne	[3.80×10^{1}]	^{41}Ca	(unstable)	^{56}Fe	1.59×10^{5}
^{22}Ne	2.25×10^{4}	^{42}Ca	[2.17]	^{57}Fe	[5.35×10^{3}]
^{23}Na	1.03×10^{4}	^{43}Ca	[4.95×10^{-1}]	^{58}Fe	[8.07×10^{2}]
^{24}Mg	1.46×10^{5}	^{44}Ca	[7.01]	^{60}Fe	(unstable)
^{25}Mg	2.51×10^{4}	^{46}Ca	[1.12×10^{-1}]	^{57}Co	(unstable)
^{26}Mg	3.21×10^{4}	^{48}Ca	[6.30×10^{-1}]	^{59}Co	[2.77×10^{2}]
^{26}Al	(unstable)	^{45}Sc	[1.68×10^{-1}]	^{56}Ni	(unstable)
^{27}Al	1.80×10^{4}	^{44}Ti	(unstable)	^{58}Ni	7.38×10^{3}
^{28}Si	1.82×10^{5}	^{46}Ti	[1.03]	^{59}Ni	(unstable)
^{29}Si	8.43×10^{3}	^{47}Ti	[9.51×10^{-1}]	^{60}Ni	2.71×10^{3}

NOTES.—"(unstable)" means that source abundances of unstable species are fixed at zero. Brackets mean that cross-section errors obscure the abundances of some secondaries. They are not significant.

from a theoretical description of shock distribution in the ISM. Since $f(\mu)$ is obtained independently of the data compilation and no attempt has been made to optimize it here, it is also considered a fixed parameter.

TABLE 4

STANDARD LEAKY-BOX MODEL

Parameter	$\mu = 0$
Γ	−2.36
κ	1.18
λ_e	5.64
ε	−0.562
R_c	5.3
ν	0.97
λ_a	...
α	...
Fit	702

The main results of our investigation are summarized in Tables 4–7. The tables show the values of all astrophysical parameters except the ISM density. The tables also show the goodness-of-fit measure. Goodness of fit is plotted for each of the models in Figure 4.

It is immediately apparent from Figure 4 that none of the DRAC models with $\mu \leq 3$ leads to a satisfactory data fit. Strong shocks broaden the peak of secondary-to-primary ratios and distort the pure power-law form above 2 GeV nucleon^{-1} (Fig. 5). The DRAC models that assume exclusively strong shocks, i.e. a small value for all the exponents μ, do not provide a satisfactory fit to the data. This conclusion is consistent with earlier results that continuous acceleration by strong shocks is not consistent with cosmic-ray secondary-to-primary ratios (Eichler 1980). Henceforth we consider only models consisting predominantly of weak shocks.

DRAC model 1 does not represent the data as well as the standard model. For all shock strengths the fit was poor. It is

TABLE 5

DISTRIBUTED REACCELERATION MODEL 1

Parameter	$\mu = 3.5$	$\mu = 4$	$\mu = 5$	$\mu = 6$	$\mu = 7$	$\mu = 8$
Γ	−2.25	−2.27	−2.36	−2.35	−2.35	−2.36
κ	−0.28	−0.22	0.04	−0.10	0.10	0.08
λ_e	3.38	3.52	3.80	4.06	4.48	5.02
ε	−0.622	−0.572	−0.538	−0.508	−0.532	−0.560
R_c	...	...	...	...	...	...
ν	...	...	...	...	...	...
λ_a	8.60	7.40	5.70	4.70	3.80	3.10
α	...	...	...	...	...	...
Fit	943	872	794	761	740	730

TABLE 6

DISTRIBUTED REACCELERATION MODEL 2

Parameter	$\mu = 3$	$\mu = 3.5$	$\mu = 4$	$\mu = 5$	$\mu = 6$	$\mu = 7$	$\mu = 8$	$f(\mu)$
Γ	−2.24	−2.30	−2.33	−2.35	−2.36	−2.36	−2.36	−2.32
κ	...	...	...	...	...	...	...	...
λ_e	3.40	3.56	3.60	3.78	3.94	4.26	4.70	3.84
ε	−0.540	−0.442	−0.420	−0.386	−0.404	−0.452	−0.500	−0.468
R_c	...	...	...	...	...	...	...	...
ν	...	...	...	...	...	...	...	...
λ_a	21.4	24.4	17.1	12.6	8.2	5.7	4.5	11.6
α	0.55	0.75	0.65	0.66	0.54	0.39	0.33	0.72
Fit	896	779	737	708	695	686	685	727

TABLE 7

DISTRIBUTED REACCELERATION MODEL 3

Parameter	$\mu = 3$	$\mu = 3.5$	$\mu = 4$	$\mu = 5$	$\mu = 6$	$\mu = 7$	$\mu = 8$	$f(\mu)$
Γ	−2.25	−2.32	−2.34	−2.36	−2.36	−2.37	−2.37	−2.36
κ	1.28	1.30	1.16	0.66	0.80	0.86	0.38	1.10
λ_e	3.60	3.74	3.82	3.86	4.14	4.44	4.70	4.06
ε	−0.550	−0.446	−0.432	−0.422	−0.444	−0.470	−0.492	−0.492
R_c	...	...	...	...	...	...	...	...
ν	...	...	...	...	...	...	...	...
λ_a	23.6	29.8	21.7	12.1	9.0	7.2	5.6	12.0
α	0.69	0.96	0.83	0.63	0.55	0.49	0.45	0.71
Fit	810	713	691	679	671	669	672	686

also clear that a distribution of shock strengths cannot improve the situation. Model 1 differs from other DRAC models because the amount of shock acceleration is *independent* of energy. The rate of encounter with shocks and the momentum boost multiple from a shock interaction are the same at all energies. These circumstances are ruled out in our analysis. It is noteworthy that DRAC model 1 has fewer free parameters than the standard leaky-box model.

DRAC models 2 and 3 fit the data as well as or better than the standard model for sufficiently weak shocks. Model 2 requires only five free parameters, one fewer than the standard model, and fits well when $\mu > 4$. Model 3 requires six free parameters, the same as the standard model, and fits better than the standard model when $\mu > 3.5$. Both results show that DRAC models reproduce the observational data with as many or fewer parameters than the standard model. Model 2 is completely free of the ad hoc parameters described in § 2; model 3 retains the flattening of the source spectrum, κ. Both models use a simple power law in rigidity for the mean escape path length.

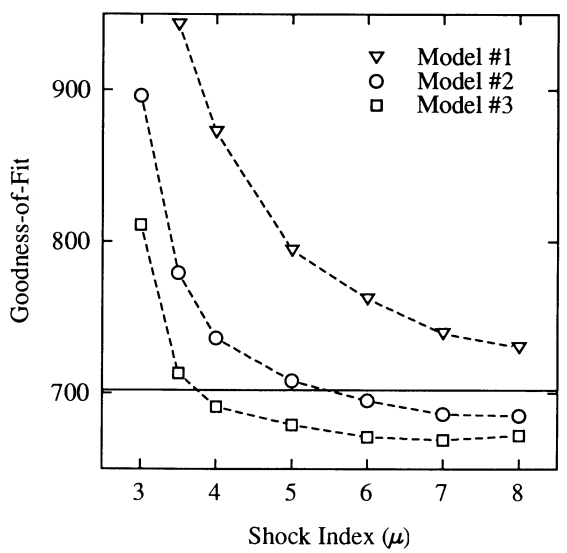

FIG. 4.—Comparison of goodness of fit of the three distributed reacceleration models to observational data with standard model fit (*solid line*).

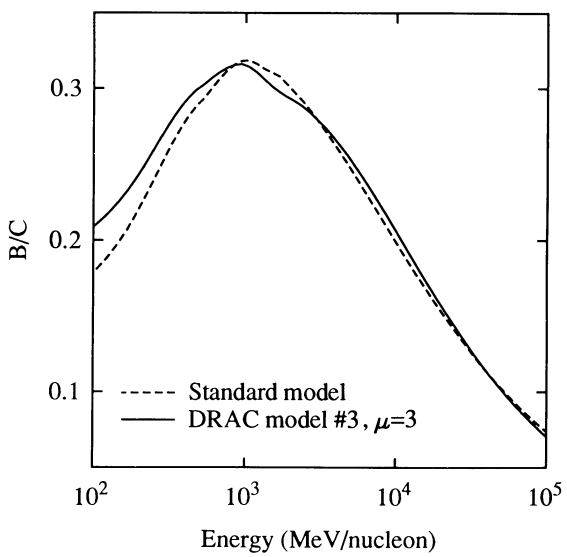

FIG. 5.—Comparison of the boron/carbon ratio predicted by the standard leaky-box model (*dashed line*) and distributed reacceleration model 3 ($\mu = 3$) outside the heliosphere. The DRAC model shown is an example of a *poor* fit caused by relatively strong shock reacceleration.

Variations in DRAC model parameters with shock strength μ demonstrate the general features of reacceleration. Consider the acceptable models 2 and 3 with $\mu \geq 3.5$ (Tables 6 and 7). The optimum mean path length between shock encounters is much greater for strong shocks, i.e., many very weak shocks are more consistent with observations than a few stronger reacceleration shocks. The rigidity dependence is flatter for weaker shocks, implying that they engender less distortion of the pure power-law spectrum at high energy.

For weak shocks the deduced source spectrum indices, Γ, are nearly the same as in the standard model. For strong shocks the source spectrum is slightly flatter because reacceleration causes a slight steepening. The spectral flattening factor κ in model 3 is nearly 1, as in the standard model.

The mean path length for escape in DRAC models increases for weaker shocks but is always less than in the standard model. More rapid escape is balanced by additional particles accelerated from lower energies. The exponent of rigidity dependence, $|\varepsilon|$, is smaller and rigidity dependence is flatter in DRAC models. In standard models, rigidity dependence fully accounts for the decline in secondary-to-primary ratios with increasing energy. In DRAC models reacceleration contributes to the decline.

As discussed above, a realistic DRAC model uses a distribution of shock strengths, $f(\mu)$, rather than a single value. An appropriate distribution may be derived using shock acceleration theory if one makes specific assumptions about the rate of supernovae in the Galaxy; the evolution of supernova remnants; and the density, temperature, and magnetic field characteristics of the ISM. We have adopted the distribution deduced by Axford (1981). An interesting feature of the distribution is that only a small volume of space (less than 4%) is occupied by shocks with $\mu < 3$. Axford's distribution is approximated for use in our numerical computations by the fractions shown in Table 8. Results of the transport computations are shown in Tables 6 and 7.

With a distribution of shock strengths, both DRAC models 2 and 3 are excellent fits to the cosmic-ray observations; model 3 is slightly better than the standard model, and model 2 is slightly worse. Model 2 requires one fewer parameter than the other models.

Figure 6 compares the B/C ratio for the three models outside the heliosphere. In the region from 100 MeV nucleon^{-1} to 100 GeV nucleon^{-1} the predictions are effectively identical. Differences below a few hundred MeV nucleon^{-1} are obscured by solar modulation in the heliosphere. Above 50 GeV nucleon^{-1} the DRAC models are flatter than the standard model; the B/C ratio is 50% greater at 500 GeV nucleon^{-1}. The high-energy behavior has also been described by Wandel (1990).

Figure 7 shows the B/C ratio for three models inside the heliosphere with force-field modulation of 300 MV. The results

TABLE 8

SHOCK-STRENGTH DISTRIBUTION $f(\mu)$

Shock Strength (μ)	Fraction in ISM
2.3	0.02
3.0	0.08
4.0	0.10
5.0	0.10
6.0	0.10
7.0	0.10
$\geq$8.0	0.50

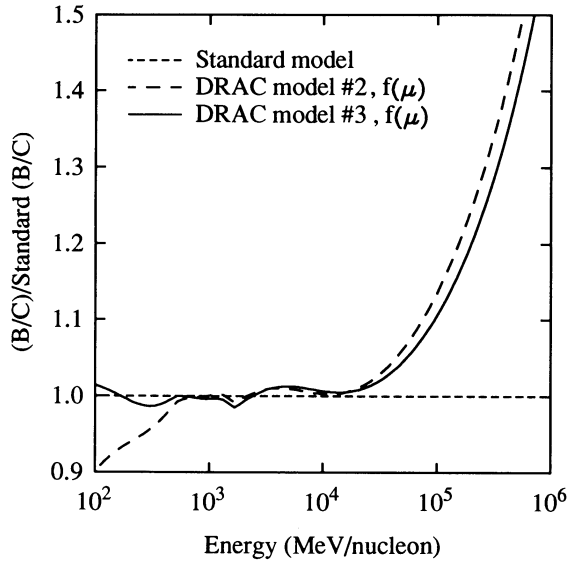

FIG. 6.—Comparison of the boron/carbon ratio predicted by the standard leaky-box models and DRAC models 2 and 3 with shock distribution $f(\mu)$ outside the heliosphere. Results are shown as a ratio to the standard model result.

are compared with data from the compilation which were collected during varying phases of the solar cycle. The agreement of all models with data is satisfactory. Note, however, that $\chi^2/\mathrm{DOF} \approx 1$ cannot be attained because data from Engelmann et al. (1990) and Gupta & Webber (1989) differ systematically by about 3 standard deviations. Above 50 GeV nucleon^{-1} the DRAC models predict somewhat greater B/C ratios, but available data in that range are not sufficiently precise to test the models.

Figure 8 shows the ratio of sub-iron elements ($21 \leq Z \leq 24$) to iron in three models inside the heliosphere with force-field modulation of 300 MV. The results are compared with data from the compilation which were collected during varying

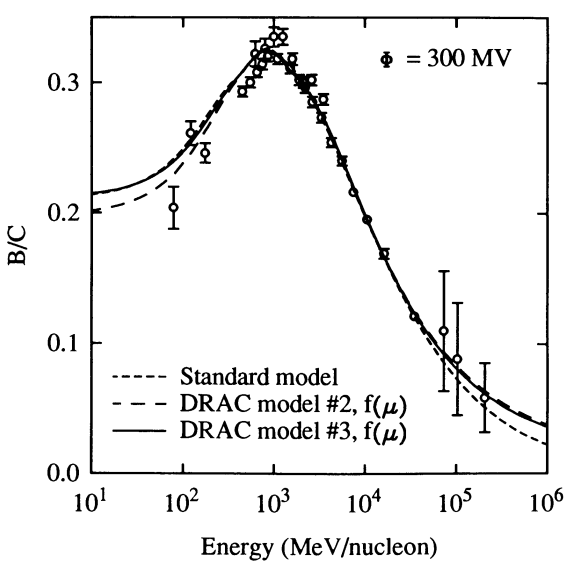

FIG. 7.—Comparison of the boron/carbon ratio predicted by the three transport models with data from the observation compilation. Model predictions are modulated to 300 MV using the force-field approximation.

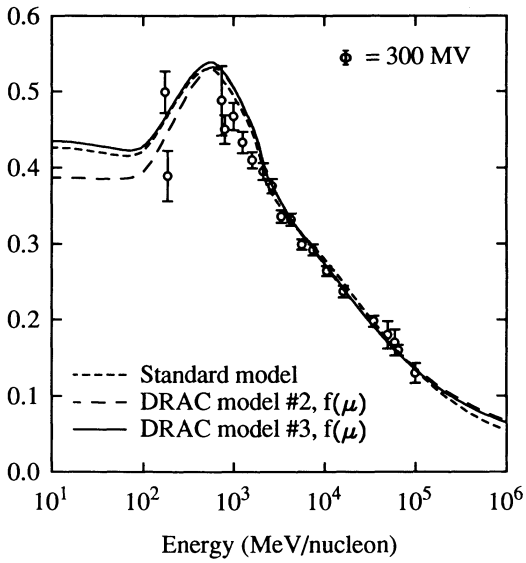

FIG. 8.—Comparison of the sub-iron/iron predicted by the three transport models with data from the observational compilation. Model predictions are modulated to 300 MV using the force-field approximation.

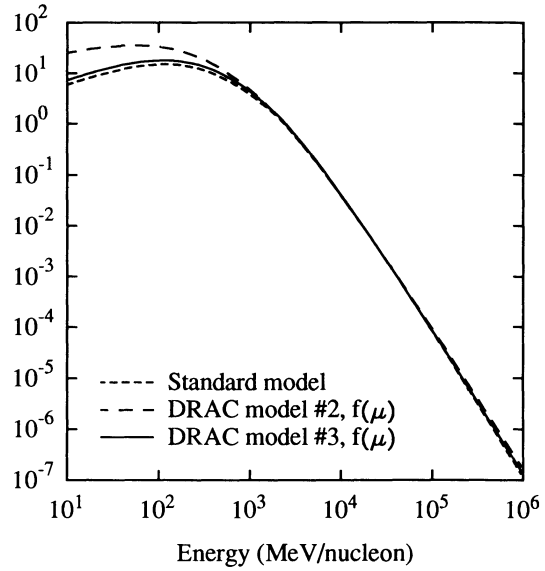

FIG. 9.—Comparison of the absolute oxygen spectra predicted by the standard leaky-box models and DRAC models 2 and 3 with shock distribution $f(\mu)$ outside the heliosphere. Spectrum units are arbitrary.

phases of the solar cycle. The agreement of all models with data is satisfactory. Relatively minor discrepancies around 1 GeV nucleon^{-1} are probably caused by cross-section errors.

Semiempirical cross-section formulae were used uncritically throughout this analysis over the entire energy range. The formulas are generally accurate to 20%–30% above 100 MeV, and are sometimes valid down to 50 MeV. Low-energy cross sections (less than 100 MeV) are particularly important for studying compositional anomalies in DRAC models (Silberberg et al. 1983). We have not yet attempted to include low-energy cross-section measurements in the semiempirical formulae, and hence we are unable to comment on this aspect of DRAC models. Identical cross sections have been used in all transport computations presented here, maintaining a consistent environment for comparing the models.

Figure 9 shows the shape of the cosmic-ray oxygen spectrum outside the heliosphere for three models. The standard leaky-box model and DRAC model 3 are nearly identical. Model 2, which does not have source spectrum flattering, is up to a factor of 3 larger at low energies. Energies below a few hundred MeV nucleon^{-1} are obscured by solar modulation. All spectra are consistent with observations.

The cosmic-ray confinement time is a function of the escape path length and ISM density. Figure 10 shows the confinement time for three models. The confinement time is around 10^7 yr for most cosmic radiation in the standard leaky-box model. Constant confinement times in the standard model arise from the mean–path-length rigidity independence, which is eliminated in DRAC models. In DRAC models the confinement time is roughly a power law in energy. DRAC model confinement times are up to 10 times greater than the standard model below $E \leq 1$ GeV nucleon^{-1}.

Figure 11 shows the nominal number of shocks encountered by cosmic-ray nuclei at each energy. The function was deduced by dividing the rigidity-dependent mean escape path length by the rigidity-dependent mean reacceleration path length. The actual number of shocks encountered by a particle depends on its transport history. The function shown is the lower limit for an arriving particle whose energy has not been significantly affected by ionization loss.

5. CONCLUSIONS AND INTERPRETATION

The results presented in § 4 demonstrate that distributed reacceleration (DRAC) models are a viable interpretation of Galactic cosmic-ray transport. The models reproduce cosmic-ray observations in the same detail and with the same accuracy as standard leaky-box models. DRAC models require the same number (or fewer) of adjustable parameters as standard leaky-box models. Some of the ad hoc fitting parameters used in standard models are replaced by shock acceleration parameters which have a direct astrophysical significance indepen-

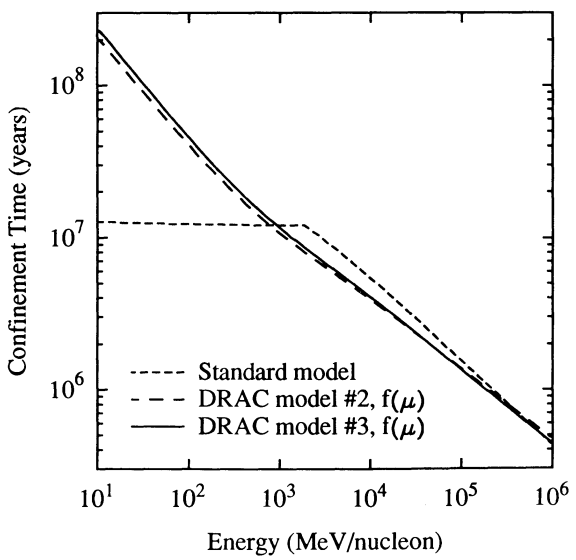

FIG. 10.—Mean cosmic-ray confinement time as a function of energy for the standard leaky-box models and DRAC models 2 and 3 with shock distribution $f(\mu)$.

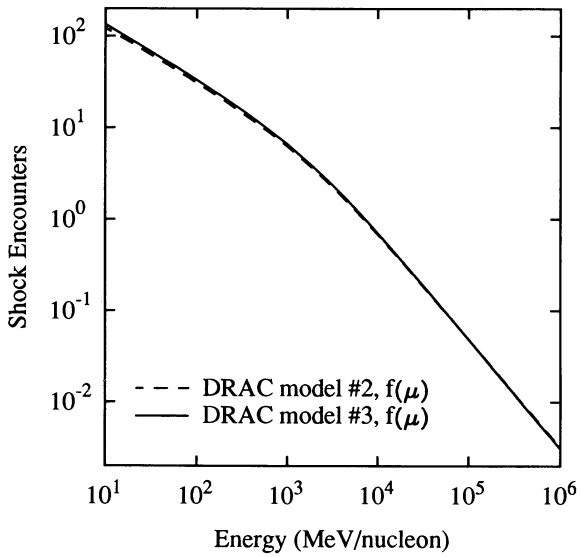

FIG. 11.—Average number of shock encounters during the confinement lifetime of a cosmic-ray primary in the distributed reacceleration models. For cosmic-ray secondaries the number of encounters is twice as high.

dent of the cosmic-ray data. Reacceleration of cosmic radiation in the hot ISM is expected (Cesarsky 1987; Giler et al. 1987). We have shown that DRAC models provide a satisfactory approach to incorporating reacceleration into standard cosmic-ray data analysis.

DRAC models explain the peak in the B/C ratio, and other secondary-to-primary ratios, around 1 GeV nucleon^{-1}. Reacceleration promotes older, low-energy secondaries more than younger, low-energy primaries, causing a buildup at energies just below the point where acceleration ceases to dominate transport (about 5 GeV nucleon^{-1}). In contrast, the standard leaky-box model is fitted to the B/C ratio by adjusting the mean path length to be energy-independent below a few GeV nucleon^{-1}. As shown in Figure 7, standard leaky-box and DRAC models agree with the wide range of observations of the B/C ratio.

At very high energies approaching 1 TeV nucleon^{-1} or more, DRAC models predict that the B/C ratio is at least 50% greater than that in the standard model. The additional particles are the exponential tail of much lower energy boron ions which have received extraordinary energy boosts during reacceleration. This behavior agrees with our previous conclusions (Wandel et al. 1987).

DRAC model results with fixed shock strength (μ) allow us to infer the ISM conditions that are consistent with cosmic-ray observations. DRAC model 1 fails because the mean path length between reacceleration shocks is independent of energy. This failure demonstrates that reaccelerations in the ISM must be energy-dependent, that is, high-energy particles must be reaccelerated by shocks at a lower rate or less efficiently than low-energy particles. One scenario for this behavior is that high-energy cosmic rays escape from shock entrainment more easily than low-energy cosmic rays. "Effective" encounters for high-energy particles are therefore rare. Such behavior is consistent with the declining diffusion coefficient for scattering by magnetic irregularities that is predicted above 10 GeV nucleon^{-1} (Cesarsky & Lagage 1981; Ginzburg & Ptuskin 1981).

All DRAC models with $\mu \leq 3$ are unsatisfactory. Multiple encounters with strong shocks are not compatible with the cosmic-ray observations. Ions are promoted from the source material pool to cosmic-ray "status" when they are first accelerated to cosmic-ray energies, probably by shock mechanisms. Thereafter, our results indicate that very few (less than 5%) cosmic rays are reaccelerated by strong shocks. We infer that only a small percentage of interstellar space can be filled with very strong shocks ($\mu \approx 2.3$). The exact fraction depends on the relative contributions of diffusion and convection to transport.

Realistic DRAC models with a distribution of shock strengths $f(\mu)$ yield additional information about the conditions of cosmic-ray transport in the ISM. The mean path length for escape decreases with energy, while the mean path length between reacceleration events increases with energy, though somewhat more slowly. In DRAC models the ratio of the escape path length to that for shock encounters varies from about 100 at 10 MeV nucleon^{-1} to less than 0.01 at 1 TeV nucleon^{-1} (Fig. 11). At 7 GeV nucleon^{-1} an average of one shock encounter occurs prior to escape. This transition causes the peak in secondary-to-primary ratios just below that energy. Low-energy particles are pushed into the GeV nucleon^{-1} range by many reacceleration events over their lifetime, but higher energy particles suffer few, if any, shocks which can move them out of that range.

The exponent of rigidity-dependent escape in DRAC models is between -0.47 and -0.49, as opposed to the significantly steeper -0.56 in the standard model. This prediction is somewhat closer to the value of -0.33 predicted by the Kolmogorov theory of diffusion in turbulent fields. A strong rigidity dependence of escape path length (above 10 GeV nucleon^{-1}) implies a strong energy dependence of anisotropy, which is contrary to observations (Ptuskin 1991). Our results have a flatter rigidity dependence, helping to reduce the discrepancy between anisotropy and escape.

The impetus for distributed acceleration was to explain isotopic anomalies in cosmic-ray data at low energy (Silberberg et al. 1983). Low-energy proton-nucleus reactions have fewer channels and greater cross sections than high-energy reactions. A major limitation of the current analysis is the lack of an organized cross-section model between 10 and 100 MeV nucleon^{-1}. Low-energy cosmic rays have confinement times approaching 10^8 yr (Fig. 10) and suffer up to 100 reaccelerations prior to observation (Fig. 11). There is therefore a strong possibility that characteristics of low-energy reactions are translated to higher energies in DRAC models.

The authors gratefully acknowledge support from the Office of Naval Research and NASA (DPR W17681). The work of J. R. L. was partially funded by SFA, Inc., under contract N00014-89-C-2285 and by Bendix Field Engineering Corporation under contract N00014-89-C-2103 with the Naval Research Laboratory.

REFERENCES

Axford, W. I. 1981, Proc. 17th Int. Cosmic Ray Conf. (Paris), 12, 155
Binns, W. R., Garrard, T. L., Israel, M. H., Jones, M. D., Kamionkowski, M. P., Klarmann, J., Stone, E. C., & Waddington, C. J. 1988, ApJ, 324, 1106
Blandford, R. D., & Ostriker, J. P. 1980, ApJ, 237, 793
Cesarsky, C. J. 1987, Proc. 20th Int. Cosmic Ray Conf. (Moscow), 7, 87
Cesarsky, C. J., & Lagage, P. O. 1981, Proc. 17th Int. Cosmic Ray Conf. (Paris), 2, 335
Cowsik, R. 1986, A&A, 155, 344

Eichler, D. 1980, ApJ, 237, 809
Engelmann, J. J., et al. 1990, A&A, 233, 96
Ferrando, P., et al. 1988, A&A, 193, 69
Ferrando, P., Lal, N., McDonald, F. B., & Webber, W. R. 1991, A&A, 247, 163
Fisk, L. A. 1971, J. Geophys. Res. 76, 221
Garcia-Munoz, M., Margolis, S. H., Simpson, J. A., & Wefel, J. P. 1979, Proc. 16th Int. Cosmic Ray Conf. (Kyoto), 1, 310
Garcia-Munoz, M., & Simpson, J. A. 1979, Proc. 16th Int. Cosmic Ray Conf. (Kyoto), 1, 270
Garcia-Munoz, M., Simpson, J. A., & Wefel, J. P. 1981, Proc. 17th Int. Cosmic Ray Conf. (Paris), 2, 72
Giler, M., Osborne, D. L., Szabelska, B., Wdowczyk, J., & Wolfendale, A. W. 1987, Proc. 20th Int. Cosmic Ray Conf. (Moscow), 2, 214
Ginzburg, V. L., & Ptuskin, V. S. 1981, Proc. 17th Int. Cosmic Ray Conf. (Paris), 2, 336
Ginzburg, V. L., & Syrovatskii, S. I. 1964, The Origin of Cosmic Rays (New York: Macmillan)
Gleeson, L. J., & Axford, W. I. 1968, ApJ, 154, 1011
Gupta, M., & Webber, W. R. 1989, ApJ, 340, 1124
Jokipii, J. R. 1976, ApJ, 208, 900
Jones, F. C. 1979, ApJ, 229, 747
———. 1991, Proc. 22d Int. Cosmic Ray Conf. (Dublin), 2, 268
Krombel, K. E., & Wiedenbeck, M. E. 1985, Proc. 19th Int. Cosmic Ray Conf. (La Jolla), 2, 92
———. 1988, ApJ, 328, 940
Leske, R. A., Milliken, B., & Wiedenbeck, M. E. 1992, ApJ, 390, L99
Letaw, J. R. 1992, SRA Rep. 92-02, CTX 2.0: Code Summary (Annapolis: Space Radiation Associates)
Letaw, J. R., Adams, J. H., Silberberg, R., & Tsao, C. H. 1985, Ap&SS, 114, 365
Letaw, J. R., & Roginsky, J. 1989, SCC Report 89-01, Equations of Cosmic-Ray Transport with Distributed Acceleration (Millersville: Severn Communications Corp.)
Letaw, J. R., Silberberg, R., & Tsao, C. H. 1984, ApJS, 56, 369
Lezniak, J. A. 1979, Ap&SS, 63, 279
Muller, D., Swordy, S. P., Meyer, P., L'Heureux, J., & Grunsfeld, J. M. 1991, ApJ, 374, 356
Press, W. H., Flannery, B. P., Teukolsky, S. A., & Vetterling, W. T. 1986, Numerical Recipes (Cambridge: Cambridge Univ. Press)
Ptuskin, V. S. 1991, in Cosmic Rays, Supernovae and the Interstellar Medium, ed. M. M. Shapiro (Dordrecht: Kluwer), 119
Silberberg, R., Tsao, C. H., Letaw, J. R., & Shapiro, M. M. 1983, Phys. Rev. Lett., 51, 1217
Simon, M., Heinrich, W., & Mathis, K. D. 1986, ApJ, 300, 31
Stephens, S. A. 1990, Proc. 21st Int. Cosmic Ray Conf. (Adelaide), 7, 241
Swordy, S. P., Muller, D., Meyer, P., L'Heureux, J., & Grunsfeld, J. 1990, ApJ, 349, 625
Wandel, A. 1990, Proc. 21st Int. Cosmic Ray Conf. (Adelaide), 3, 357
Wandel, A., Eichler, D., Letaw, J. R., Silberberg, R., & Tsao, C. H. 1987, ApJ, 316, 676
Webber, W. R. 1981, Proc. 17th Int. Cosmic Ray Conf. (Paris), 2, 80
Webber, W. R., Kish, J. C., & Schrier, D. A. 1985, Proc. 19th Int. Cosmic Ray Conf. (La Jolla), 2, 88
Wiedenbeck, M. E. 1983, Proc. 18th Int. Cosmic Ray Conf. (Bangalore), 9, 147
———. 1985, Proc. 19th Int. Cosmic Ray Conf. (La Jolla), 2, 84
Wiedenbeck, M. E., & Greiner, D. E. 1980, ApJ, 239, L139